Original Research

Integration of "omics" techniques: Dronedarone affects cardiac remodeling in the infarction border zone

Ravi K Chilukoti[1,*], Josefine Lendeckel[1,*], Katrin Darm[2], Alicja Bukowska[3], Andreas Goette[3,4], Marc Sühling[1], Kirsten Utpatel[5], Barbara Peters[6], Georg Homuth[7], Uwe Völker[7], Carmen Wolke[1], Christian Scharf[2] and Uwe Lendeckel[1]

[1]Institute of Medical Biochemistry and Molecular Biology, University Medicine Greifswald, Greifswald D-17475, Germany; [2]Department of Otorhinolaryngology, Head and Neck Surgery, University Medicine Greifswald, Greifswald D-17475, Germany; [3]Working Group: Molecular Electrophysiology, Otto-von-Guericke University, University Hospital Magdeburg, Magdeburg D-39120, Germany; [4]Department of Cardiology and Intensive Care Medicine, St. Vincenz-Hospital, Paderborn D-33098, Germany; [5]Department of Pathology, University Medicine Greifswald, Greifswald D-17475, Germany; [6]Institute of Physiology, University Medicine Greifswald, Karlsburg D-17495, Germany; [7]Interfaculty Institute for Genetics and Functional Genomics, University Medicine Greifswald, D-17475 Greifswald, Germany
[*]These authors contributed equally to this work.
Corresponding author: Uwe Lendeckel. Email: uwe.lendeckel@uni-greifswald.de

Impact statement

Dronedarone reduced the infarct size in models of acute myocardial infarction (MI).

Here, we show that dronedarone attenuates many of the substantial changes in gene expression that are provoked by acute myocardial infarction (AMI) in pigs. Dronedarone modifies the expression of gene panels related to post-infarction cardiac healing and remodeling processes and, most remarkably, this occurs predominantly in the infarction border-zone and much less so in the vital or infarcted myocardium. Combined "omics" identified matricellular proteins and ECM as major dronedarone-regulated targets and emphasizes their relevance for Disease Charts and Tox Function Charts associated with tissue remodeling and cellular movement.

The results demonstrate dronedarone's capability of regulating cardiac repair and remodeling processes specifically in the infarction border zone and identify underlying mechanisms and pathways that might be employed in future therapeutic strategies to improve long-term cardiac tissue function and stability.

Abstract

Dronedarone improves microvascular flow during atrial fibrillation and reduces the infarct size in acute models of myocardial infarction. However, dronedarone might be harmful in patients with recent decompensated heart failure and increases mortality in patients with permanent atrial fibrillation. A pathophysiological explanation for these discrepant data is lacking. This study investigated the effects of dronedarone on gene and protein expression in the infarcted area and border zone in pigs subjected to anterior ischemia/reperfusion myocardial infarction. The ischemia/reperfusion myocardial infarction was induced in 16 pigs. Eight pigs were treated with dronedarone for 28 days after myocardial infarction, the remaining pigs served as control. Microarray-based transcriptome profiling and 2D-DIGE-based proteome analysis were used to assess the effects of dronedarone on left ventricular gene expression in healthy (LV), infarcted (MI), and border zone tissue. Selected targets were validated by RT-qPCR or immunoblot analyses, with special emphasize given to the transcriptome/proteome overlap. Combined "omics" analysis was performed to identify most significant disease and function charts affected by dronedarone and to establish an integrated network. The levels of 879 (BZ) or 7 (MI) transcripts and 51 (LV) or 15 (BZ) proteins were significantly altered by dronedarone, pointing to a substantial efficacy of dronedarone in the border zone. Transcriptome and proteome data indicate that dronedarone influences post-infarction remodeling processes and identify matricellular proteins as major targets of dronedarone in this setting. This finding is fully supported by the disease and function charts as well as by the integrated network established by combined "omics". Dronedarone therapy alters myocardial gene expression after acute myocardial infarction with pronounced effects in the border zone. Dronedarone promotes infarct healing via regulation of periostin and might contribute to the limitation of its expansion as well as cardiac rupture. Thus, there are no experimental hints that dronedarone per se has direct harmful effects after MI in ventricular tissue.

Keywords: Acute myocardial infarction, cardiac healing and remodeling, dronedarone matricellular proteins, integrated omics

Experimental Biology and Medicine **2018; 243: 895–910. DOI: 10.1177/1535370218788517**

Introduction

Dronedarone is an antiarrhythmic drug for treatment of atrial fibrillation (AF). Data from the ATHENA (a placebo-controlled, double-blind, parallel arm trial to assess the efficacy of dronedarone 400 mg bid for the prevention of cardiovascular hospitalization or death from any cause in patients with AF/atrial flutter) study showed that dronedarone therapy reduces cardiovascular mortality, hospitalization, and incidence of myocardial infarction in patients with AF.[1] The incidence of acute coronary syndromes was also reduced in patients with coronary artery disease (CAD) at baseline as a subgroup analyses revealed.[2] However, dronedarone has been shown to be harmful in patients with recent decompensated heart failure,[3] and according to the PALLAS (permanent AF outcome study using dronedarone on top of standard therapy) study, dronedarone therapy increases mortality in patients with permanent AF, and doubles the rate of the first composite co-primary outcome such as stroke, myocardial infarction, and systemic embolism in these particular patients.[4] In line with their increased risk for subsequent ischemic events,[5] AF patients exhibit a reduced coronary flow reserve (CFR).[6,7] Benzofuran derivatives such as dronedarone (or amiodarone) have been shown to increase coronary flow[8,9] and to largely prevent the AF-dependent decline of the CFR during acute RAP *in vivo*.[10] Dronedarone also reduced the infarct size in models of acute myocardial infarct (MI) in pigs as well as of cerebral infarct in rat.[11,12]

The aim of this study was to elucidate in a model of ischemia/reperfusion myocardial infarction in pigs the effects of dronedarone on the transcriptome and proteome of healthy, infarcted, and border-zone myocardium after 28 days of recovery. Furthermore, an integrated "omics" approach was applied to identify (in a hypothesis-free and unbiased manner) molecular targets and pathways that underlie dronedarone-mediated effects on infarcted, border-zone, or healthy tissue.

Methods

Acute myocardial infarction model

All animal care and experimental procedures were approved by the Landesverwaltungsamt Sachsen-Anhalt (Az42502–2-1117-IMTR); 16 pigs were subjected to anterior ischemia/reperfusion MI as described in detail recently.[13] Eight pigs were treated with dronedarone for four weeks after MI, the remaining pigs served as control. At day 28, tissue samples were taken from healthy left ventricular (LV) and right ventricular (RV) myocardium as well as from LV myocardium from the infarct area (MI) or the border zone (BZ). Tissue samples from untreated pigs were designated accordingly as LV, RV, MI or BZ, whereas those obtained from dronedarone-treated pigs were designated LV-D, RV-D, MI-D, or BZ-D, respectively. Designation of samples and sites of sample collection are illustrated in Figure 1. Tissue samples were immediately frozen in liquid nitrogen and used for transcriptome profiling, RT-qPCR, proteome, and immunoblot analyses as described below. The experimental design is shown in Online Supplement 8.

Microarray array expression analysis

Transcriptome analyses were performed using the GeneChip Porcine Genome Arrays (Affymetrix Inc., Santa Clara, CA, USA). Expression profiling was done at the level of single RNA samples for LV, LV-D, MI, MI-D, BZ, and BZ-D ($n = 3$ for all groups). Target preparation and hybridization were performed exactly as previously described.[10]

Microarray data and statistical analysis

Data were analyzed as described recently.[10] Significant differences in gene expression were identified using the following cut-off criteria: one-way analysis of variance with subsequent Benjamini and Hochberg false discovery rate multiple-testing correction on pair-wise comparisons, (ANOVA, $P \leq 0.05$), signal correction statistics (ratio builder, $P \leq 0.05$), and fold-change $\geq$1.5-fold (for a complete list of significantly regulated genes, see Online Supplement Table 1). The improved annotation information for porcine expressed sequences provided by Couture *et al.*[14] was used.

In silico-pathway- and functional analysis of microarray data

In-silico-pathway- and functional analysis of differentially expressed genes was carried out using the commercial systems biology oriented package Ingenuity Pathways Analysis (Ingenuity Systems, Inc. CA, USA) using the annotation details provided by Couture *et al.*[14] with their corresponding gene identifiers and expression values.

Reverse transcription quantitative PCR

Reverse transcription quantitative PCR (RT-qPCR) was applied to validate several specific candidate genes resulting from the microarray analyses. Reactions were performed as previously described.[15,16] Quantities of RPL mRNA were used to normalize cDNA contents. The specific primers applied are listed in Online Supplement 3.

Immunoblot analyses

Experiments were performed as previously described.[15,16] Twenty micrograms of protein were separated by sodium dodecyl sulfate-polyacrylamide gel electrophoresis (SDS-PAGE) and transferred to nitrocellulose membranes. The membranes were incubated with primary antibodies followed by incubation with horseradish peroxidase-conjugated secondary antibodies (used antibodies are summarized in Online Supplement 4). Enhanced chemiluminescence substrate dura (Pierce, Rockford, USA) was used for detection and the AlphaEaseFC software (AlphaImager System, Alpha Innotech, CA, USA) was applied for quantification.

Histochemistry and immunohistochemistry

Cardiac tissue was fixed in 4% neutral-buffered formalin, dehydrated and embedded in paraffin. Staining of 2-µm slides by histochemistry and immunohistochemistry was performed as follows: sections were deparaffinized with xylene and ethanol and stained with AFOG (acid fuchsin

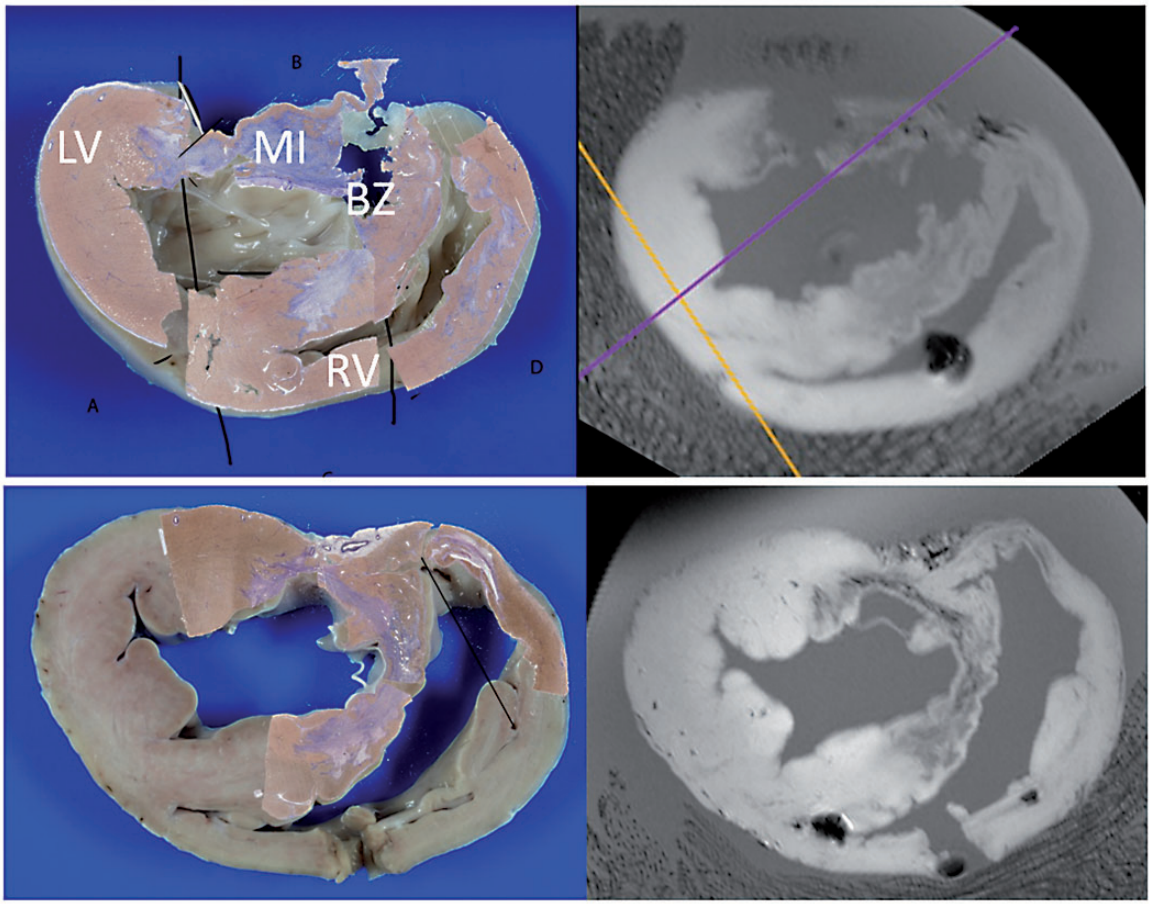

Figure 1. Macroscopic and histologic findings compared to MTI scan and assignment of samples. Photograph of a slice of a swine heart (left) with the respective AFOG-stained sections (overlaid in Adobe Photoshop) compared to the corresponding MRI image (Osirix). Prior to fixation, samples were taken from healthy left ventricular (LV), healthy right ventricular (RV), infarcted left ventricular (MI), or peri-infarct region (border-zone; BZ) tissues, respectively. The exact assignment of samples has been verified by examining the exact positions of biopsy sites the samples were taken from by (I) macroscopic and histologic analysis of swine heart tissue slices and (II) by comparing it to the corresponding MRI image from the whole heart MRI. Biopsy sites are clearly visible and allow for precise allocation of, e.g. RV (bottom) and BZ (top) samples.

orange G) according to standard protocol or treated with primary antibodies (anti-POSTN-ab polyclonal from Sigma-Aldrich, 1:200 diluted), peroxidase-conjugated secondary antibody, and diaminobenzidine substrate.

2D-DIGE coupled mass spectrometry

Two-dimensional-differential in gel electrophoresis. Comparative proteome analysis of BZ, LV, and their respective dronedarone-treated tissues were analyzed as previously described.[17] Quantified protein extracts were minimally labeled using the Refraction-2D™-kit according to the manufactures' suggestions (NH DyeAGNOSTICS GmbH, Halle/S., Germany) before electrophoresis. Individual heart protein extracts, 50 μg each ($n = 4$ per group) were labeled with 400 pmol of either G-200 or G-300 dyes. As an internal standard, aliquots of all individual samples were pooled and labeled with G-100. The labeling of the samples was done by dye swapping such that protein extracts from two animals per group were labeled with G-200 and G-300 each.

Two-dimensional gel electrophoresis was performed as previously described.[18,19]

Image analysis and statistical tests. After separation in the second dimension, the gel images were recorded on a Typhoon 9400 Scanner (GE Healthcare) and analyzed with Delta 2D software version 4.0 (Decodon, Greifswald, Germany). After matching the gels, the spot volumes were analyzed by Delta2D and the TMEV (Multi Experiment Viewer) statistic module of the same software package. Statistically significant differences in spot intensities among the groups consisting of four individual biological replicates each were calculated by one-way ANOVA applying Welch *t*-test with a *P*-value cutoff of ≤ 0.05.[20]

In-gel digestion of proteins and mass spectrometric analysis. Preparative gels were run each with 450 μg of the pooled samples. Protein spots were visualized by colloidal Coomassie staining as described in Thiele et al.[18] and images were recorded and aligned with those of analytical gels in Delta2D. The protein spots displaying significant changes were excised from the preparative gels, tryptically digested and separated with a nano-HPLC (EASY-nLC, Proxeon Biosystems A/S, Odense, Denmark) coupled with LTQ-Orbitrap-XL mass spectrometer (Thermo Electron, Bremen, Germany) as previously described.[21]

Cutted protein spots from Western blot membranes were prior washed and destained with 50% methanol and 30% acetonitrile/50 mM ammonium bicarbonate.

Identification of proteins. Identification of proteins from 2D-spots was performed via automated SORCERER/SEQUEST search (Sorcerer built 4.04, Sage-N Research Inc., Milpitas, CA, USA) against a *sus scrofa* subset of the UniProtKB/Swiss-Prot 2017_05 database with a mass tolerance of 10 ppm (1 Da for fragment ions). Proteins identified with at least two peptides throughout the whole dataset at a peptide prophet probability of 90%.[22]

Statistical analysis

Microarray data and statistical analysis are explained in detail in the microarray methods above. RT-qPCR data were analyzed statistically using the GraphPad Prism software. Data are shown as the median with 25th and 75th percentile. Comparisons between two groups were performed with unpaired *t* test and between multiple groups using two-way analysis of variance with Tukey's *post hoc* test adjusting for multiple comparisons, considering $P < 0.05$ significant.

Results

Haemodynamics and physiology

Hemodynamic parameters and infarct size have been previously described[13] and were not different between the groups. LV ejection fraction was significantly reduced by 30% in the control group (42.26 vs. 29.78%; $P = 0.012$) and 35% in the dronedarone–treated group (46.89 vs. 30.22%; $P = 0.012$) following four weeks of infarct healing.[13]

AMI-dependent transcriptome alterations in MI and BZ

Microarray-based mRNA profiling revealed that in response to AMI, there are substantial less changes in transcript levels in the BZ (639 gene specific probe sets) than in MI (3300), when compared with LV. There was an overlap of 589 probe sets with similar mRNA level alterations both in BZ and MI. Complete lists of the corresponding genes are given in Online Supplement 5, data sheets: MI, BZ, and Overlap_MI_BZ, respectively.

Impact of dronedarone on the AMI-specific transcriptome in MI and BZ

Dronedarone modified the AMI-specific transcriptome but the effects were almost exclusively confined to the BZ in which 879 gene-specific probe sets displayed altered levels in response to dronedarone treatment (BZ-D vs. BZ). Only minor effects were seen for the MI (seven gene-specific probe sets differing in level between MI-D vs. MI). For a complete list of the corresponding genes see Online Supplement 6, data sheets: MI-D vs. MI and BZ-D vs. BZ. A Voronoi tree map was generated to visualize the dronedarone-mediated transcriptome dynamics and respective functional and sub-functional categories in BZ (Figure 2(a) and (b)).

Canonical pathways altered by dronedarone in BZ and MI

Ingenuity pathway analysis (IPA) of the BZ transcriptome data identified 70 canonical signaling pathways

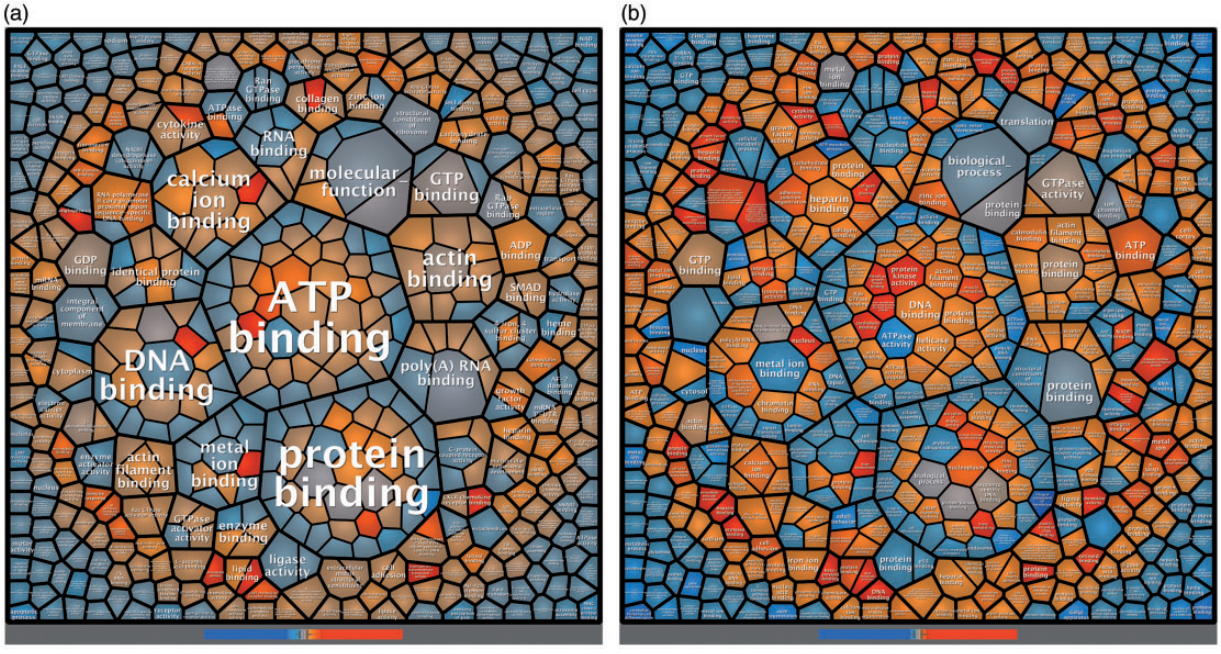

Figure 2. Voronoi treemap illustrating functional (a) and sub-functional (b) categories of dronedarone-mediated transcript level changes in the infarction border-zone, based on level 1 (a) and level 2 (b) gene ontologies, respectively. Triplicate RNA samples for each group were processed with Affymetrix porcine genome arrays and the generated data further analyzed. Improved annotations of the porcine transcriptome with all functionally annotated genes are displayed. Clustering in groups or categories means functional or systematic relationship. If a gene or a group of genes is assigned to multiple functions, it is allocated to more than one functional group and therefore appears at multiple locations within the treemap. (a) The Voronoi tree map is shown by a color ramp from dark blue (at least -10-fold repressed in BZ-D compared to BZ) via light grey (unchanged) to dark orange (at least 10-fold induced in BZ-D compared to BZ samples). (b) The Voronoi tree map is shown by a color ramp from dark blue (at least -5-fold repressed in BZ-D compared to BZ) via light grey (unchanged) to dark orange (at least 5-fold induced in BZ-D compared to BZ samples).

significantly affected by dronedarone under conditions of AMI. Pathways showing highest significance levels include ephrin receptor signaling, hepatic fibrosis signaling, PKA signaling, adherence junction signaling, integrin signaling, role of leukocytes and fibroblasts, and inhibition of matrix metalloproteases (BZ) (Online Supplement Table 5, data sheet = BZ-D vs. BZ_Direct_Pathways).

Due to the low number of significantly dronedarone-affected transcripts in MI, the overlap of MI and MI-D gene expression changes was compared to identify additional genes partially affected by dronedarone. Thereby, 624 gene-specific probe sets with similar expression change both in MI and MI-D (compared with LV), and with an additional expression change (>15%) in MI-D animals, indicating partial attenuation/aggravation by dronedarone, were identified (Online Supplement 6, data sheet = 15% Change_MI and MI-D).

IPA analysis of these partially affected genes indicated 151 significant canonical pathways (Online Supplement 7, data sheet = MI_MI-D_Pathways). Ephrin receptor signaling, PKA signaling, adherence junction signaling, integrin signaling, mitochondrial dysfunction, and NFAT in cardiac hypertrophy were among those with highest significance levels.

Dronedarone promotes post-infarction cardiac healing and remodeling in BZ

Analysis of the effects of dronedarone on the BZ transcriptome identified a panel of genes implicated in different phases of cardiac healing and remodeling. These phases include death of cardiomyocytes, acute inflammation, regression of inflammatory signals, stimulation of ECM production by cardiac fibroblasts, and formation of a mature scar. The individual phases of infarction healing and the assigned dronedarone-affected genes are shown in Figure 3(a). Although dronedarone exhibits strong effects on the corresponding transcript levels in the BZ,

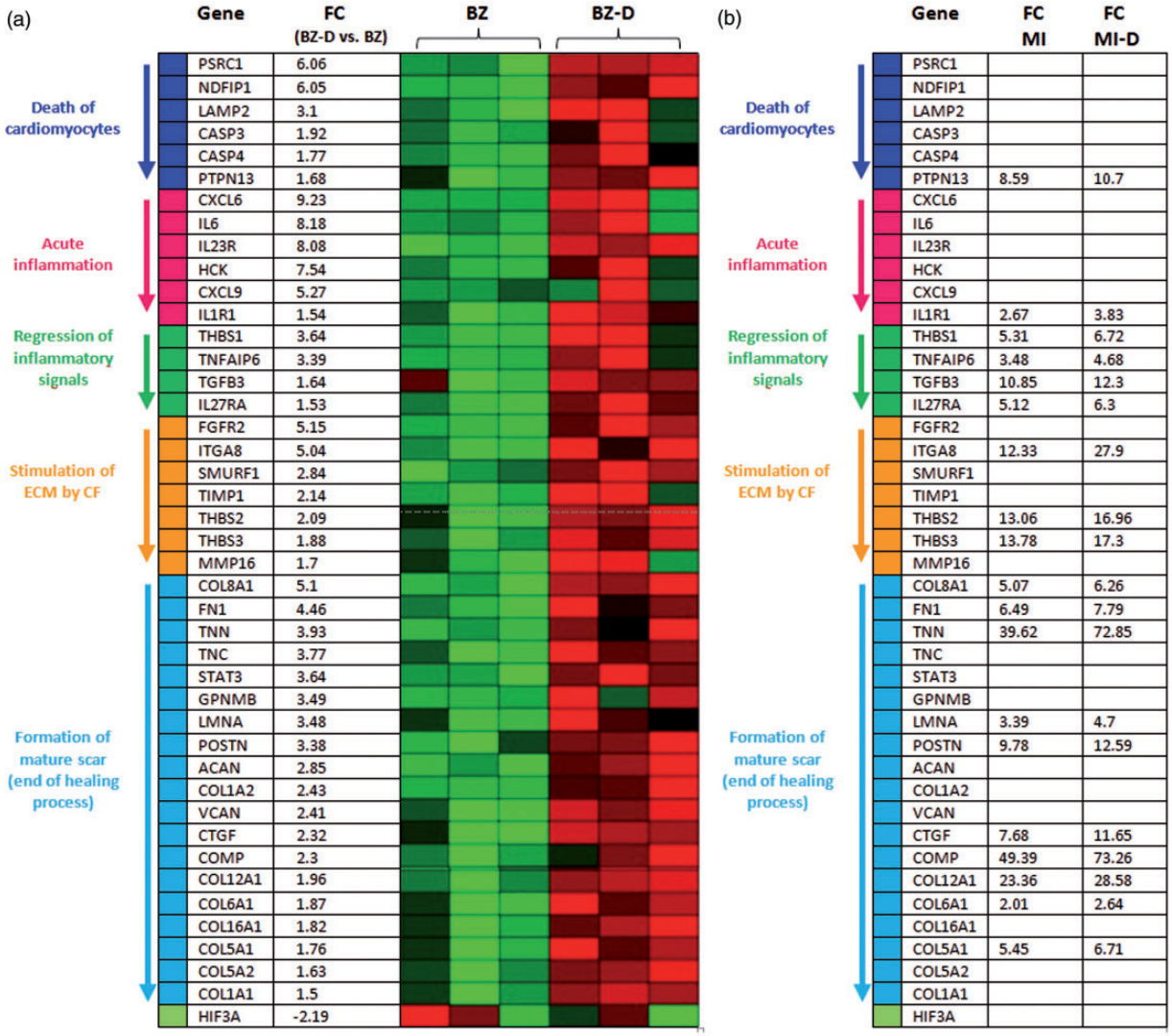

Figure 3. Heat-map displaying dronedarone-dependent differential transcript levels in different phases of post-infarction cardiac healing and remodeling. (a) Significant mRNA level alterations in infarct border zone (BZ-D vs. BZ). (b) Significant mRNA level alterations in infarct region (MI), infarct region in presence of dronedarone (MI-D), and healthy myocard (LV; left ventricle, control group). The fold change reflects alterations either in MI (MI vs. LV) or MI-D (MI-D vs. LV). The heat-map was generated using the k-NN classifier algorithm with Euclidean distance similarity measure. FC: Averaged transcript level fold change.

these were not significantly changed in MI-D compared to MI. Apparently, the impact of dronedarone on these genes is much more pronounced in the BZ compared to the MI because in the MI, a considerable fraction of these genes also showed alterations, although to a lesser extent (additional expression change >15% in MI-D; Figure 3(b)).

Impact of dronedarone on the expression of genes encoding matricellular proteins

Although all phases of infarct healing were affected by dronedarone in the BZ, the majority of dronedarone-affected genes were related to *formation of mature scar* (21/44, 47.7%), which might well reflect the late time point of analysis (28 days after AMI).

The transcript levels of a large panel of matricellular proteins were significantly altered by dronedarone: The *POSTN*-specific transcript levels were significantly increased (2.07-fold) in BZ-D (vs. BZ), and also in MI-D (9.78-fold in MI vs.12.59-fold in MI-D; = 29% additional change by dronedarone, compared to LV). The effect of dronedarone on *POSTN* in BZ could be clearly validated by RT-qPCR, as was the case for various other target genes related to infarct healing and cardiac remodeling after MI: *POSTN* (5.75-fold, $P = 0.0025$), *TGFB3* (2.32-fold, $P = 0.0215$), *THBS2* (2.45-fold, $P = 0.0215$), *THBS3* (2.12-fold, $P = 0.0405$), *FN1* (2.19-fold, $P = 0.0215$), *COL8A1* (2.77-fold, $P = 0.0504$) in BZ. In addition, a slight but non-significant dronedarone-mediated increase could be observed for *THBS1* (1.36-fold, $P = 0.2455$) and *TNC* (1.33-fold, $P = 0.1725$) mRNA levels in BZ (Figure 4). Compared to the BZ, mRNA levels appeared to be much less affected by dronedarone in the LV.

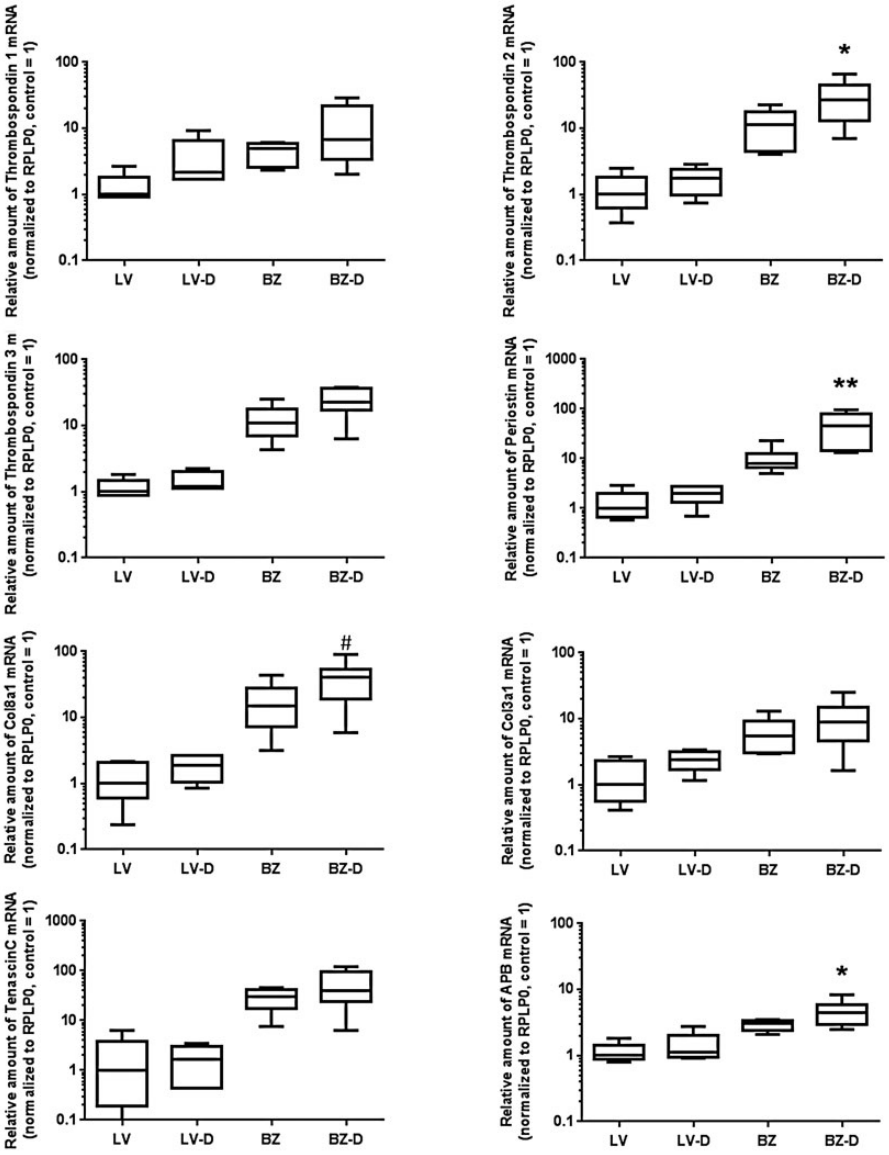

Figure 4. Validation of dronedarone-dependent mRNA level increases of *THBS-1/2/3*, *POSTN*, *TGFB3*, *FN1*, *COL8A1*, *COL3A1*, *TNC*, and APB in the BZ by RT-qPCR. The respective mRNA levels in LV (control) were set to 1. Results were given as the transcript levels in BZ, BZ-D and LV-D relative to LV (control). *RPLP0* was used as internal calibrator ($n = 4$; $^{*}P < 0.05$; $^{**}P < 0.01$; $^{\#}P = 0.0504$).

2D-DIGE coupled mass spectrometry

Altogether 2214 distinct protein spots were detected in LV/RV/BZ by 2D-DIGE experiments. Of those, the amounts of 51, 41, and 15 proteins in LV, RV, and BZ, respectively, were identified to be altered by dronedarone treatment (1.2-fold, $P < 0.05$). There was an overlap of only three proteins between LV and BZ, and of 10 proteins between LV and RV, while 1 protein was affected by dronedarone in all three tissues (Table 1).

In the BZ, as already observed in the transcriptome analyses, dronedarone provoked significant changes in the expression of genes encoding proteins associated with different phases of post-infarction cardiac healing and remodeling (Table 2). The dronedarone-affected proteins included serpin isoforms, PDIA2, CES1, isoforms of PDIA3, fatty acid-binding protein FABP4, and Ca-binding protein S100 (Figure 5). Immunoblot analysis of selected targets confirmed the observed dronedarone-mediated increase in TGFBR1, COL6A1, HSPA5, THBS1/2, RAD23A, CALD1, and POSTN protein amounts in the BZ, whereas much less expression changes could be observed in the LV (increased TGFBR1 and AT2A2) (Figure 6(a)). Remarkably, the immunoblot analyses demonstrated increased POSTN protein levels in the BZ-D as compared to BZ (Figure 6(a)). However, a similar difference could not be detected by immunostaining of cardiac tissue sections from control and dronedarone-treated pigs (Figure 6(b)). Providing a possible explanation for this apparent discrepancy, 2D-immunoblot analysis revealed distinct changes in the isoelectric point and apparent molecular weight of POSTN in response to dronedarone, which is consistent with an increased spot intensity of 95 and 68 kDa, approximately, POSTN immunoreactivity in both 1D- and 2D-immunoblot (Figure 6(c)).

Integrated omics: Compared ingenuity pathway analysis of transcriptome and proteome data

Although there has been observed a partial overlap only of proteins and transcripts differentially expressed in response to dronedarone (Table 2), the canonical pathways that have been identified by single analysis of either proteome or transcriptome data were partly identical. These common canonical pathways include hepatic fibrosis, ILK-signaling, actin cytoskeleton signaling, calcium signaling, cardiac hypertrophy signaling. In order to identify the most relevant networks and canonical pathways, an integrated approach was applied by combining transcriptome and proteome data. This led to a substantial increase of the significance level (two to six orders of magnitude) for a number of IPA *Disease* and *Tox Function Charts* (Figure 7). Among the top 10 disease charts are now skeletal and muscular disorders, cardiovascular disease, and cardiovascular system development (Figure 7(a)). With respect to Tox Function Charts, cardiac fibrosis, cardiac dysfunction, and cardiac infarction were among the top 10 that manifested as the most relevant (Figure 7(b)).

Next, to enhance the power of proposed dronedarone-affected networks, combined omics data were used to build a condensed integrated network. Of note, molecular targets identified before in *single omics approach*-derived networks – and that have already been verified in immunoblot or RT-qPCR analyses (Figures 4 and 6(a)) – reappeared in this novel integrated network (Online Supplement 1). Thereby, additional weight could be added to the relevance of verified targets such as collagens, thrombospondins, tenascin C, SERCA2 (ATP2A2), and TGFβ receptor 1 in particular. The functional association of these verified targets is illustrated in the network shown in Online Supplement 2, which again emphasizes the role of matricellular proteins and ECM as major targets of dronedarone in post AMI tissue remodeling.

Discussion

The results of the present study identify the infarction BZ as an important, if not predominant, target of dronedarone in a model of AMI. Results of transcriptome analyses implicate dronedarone in the differential expression of genes involved in various phases of cardiac healing process.[23] Data obtained from proteome analysis confirmed the rather selective effects of dronedarone on protein levels in BZ. Of the dronedarone-affected proteins in the BZ (15 proteins significantly changed (1.2-fold, $P < 0.05$), 181 changed proteins (1.2-fold, $P =$ n.s.)), 23 exhibited a similar response at transcript level. The post-infarction healing response is a complex process that involves both the infarcted and non-infarcted myocardium and is closely intertwined with ventricular remodeling, resulting in dilation, hypertrophy, and enhanced sphericity of the ventricle.[24,25] Healing of the infarcted heart comprised distinct, but partially overlapping phases: cardiomyocyte death, inflammatory phase, regression of inflammation, stimulation of ECM, and formation of mature scar. Results of our transcriptome analyses imply that 28 days after AMI there is (I) differential expression of genes that could be assigned to the different phases of infarct healing, which is (II) more pronounced in the BZ when compared to MI, and (III) which is further enhanced by dronedarone in the BZ (BZ-D). Notably, the late phase of mature scar formation appeared to be modulated by dronedarone in particular (21 of 44 genes attributed to this phase). This is in full accordance with substantial effects that dronedarone exerts on the expression of matricellular proteins and ECM, a finding that is actually reflected by the *Disease Charts* and *Tox Function Charts* actually regulated by dronedarone.

Massive loss of cardiomyocytes occurs rapidly after AMI. Nevertheless, we clearly observed effects of dronedarone on expression of genes assigned to cell death, in particular within the BZ: *PSRC1* (6.06-fold), *NDFIP1* (6.05-fold), *TNFAIP6* (3.39-fold), *LAMP2* (3.1-fold), *CASP4* (1.92-fold), *CASP3* (1.77-fold) and *PTPN13* (1.68-fold) even 28 days after infarction. This indicates that cardiac remodeling processes are still ongoing at this time point. Dronedarone had no significant efficacy in MI, but partially affected the expression of *PTPN13* (7.2% additional aggravated expression change in MI-D). Considering the well-established temporal sequence of pathomorphological changes after AMI, cell death-associated gene expression signatures observed here rather reflect cellular depletion as typically

Table 1. Proteins significantly changed by dronedarone (1.2-fold, $P < 0.05$) in LV, RV, and BZ as determined by 2D-DIGE analysis.

Only LV (38 proteins)				
Spot ID	*Gene name*	*Protein name*	*Ratio*	*P*
F1RJI7_PIG	COX6A1	Cytochrome c oxidase subunit 6A, mitochondrial	2.47	0.04
F1SN52_PIG	N/A	3-hydroxbutyryl-CoA hydrolase, mitochondrial	2.05	0.03
gi|119663043	igh	Immunglobulin heavy chain variable region, partial	0.81	0.01
gi|125987844	MYH7	Myosin heavy chain 7	0.82	0.04
gi|164511	LOC100152325	Immunglobulin lambda-like polypeptide 5	0.72	0.02
gi|335299041	LOC100156879	Cytochrom b-c 1 complex subunit 1, mitochondrial	1.20	0.04
gi|441477579	IGHG1	IgG heavy chain precursor	0.81	0.01
gi|75056480	MYH1	Myosin, heavy chain 1, skeletal muscle, adult	0.81	0.05
MYH1_PIG	MYH1	Myosin-1	0.77	0.03
Q1AG08_PIG	MYOZ2	Calsarcin 1	0.75	0.03
Q1T7A8_PIG	COL6A1	Type VI collagen alpha-1 chain	1.25	0.02
Q6J267_PIG	LGALS1	Galectin	1.21	0.05
A4UTN7_PIG	Hsph1	Heat shock 105 kDa/110 kDa protein 1	0.75	0.02
A5GFX7_PIG	CTSZ	Cathepsin Z	0.74	0.05
B5L0Y2_PIG	CAST	Calpastatin	1.23	0.01
F1RKC0_PIG	HIP1	Huntingtin interacting protein 1	0.76	0.03
F1RLP9_PIG	UBQLN4	Ubiquilin 4	0.36	0.04
F1RM45_PIG	APOE	Apolipoprotein E	0.74	0.05
F1RVG6_PIG	NEBL	Nebulette	0.73	0.04
F1S0J2_PIG	C4BPA	Complement component 4 binding protein alpha	0.77	0.03
F1S441_PIG	CANX	Calnexin	0.78	0.03
F1S5J1_PIG	LRPPRC	Leucine rich pentatricopeptide repeat containing	1.23	0.04
F1S6B5_PIG	FMOD	Fibromodulin	0.68	0.01
F1SGS6_PIG	CAPRIN1	Cell cycle associated protein 1	0.75	0.02
F1SHD7_PIG	NDUFS1	NADH:ubiquinone oxidoreductase core subunit 1	0.81	0.02
F1SID7_PIG	MYBPC3	Myosin binding protein C, cardiac	0.77	0.02
F1SM78_PIG	MRLC2	Myosin regulatory light chain 12B	1.49	0.03
F1SV04_PIG	NT5C1A	5`-nucleotidase, cytosolic IA	2.05	0.03
F2Z5B6_PIG	TPM1	Tropomyosin alpha-1 chain	1.49	0.03
GELS_PIG	GSN	Gelsolin	0.81	0.05
I3L9N1_PIG	LOC100620837	protein ADP-ribosylarginine hydrolase-like protein 1	2.05	0.03
I3LBG0_PIG	PPP4R2	Serine/Threonine-protein phosphatase 4 regulatory subunit 2	0.78	0.03
I3LDI3_PIG	IRGQ	Immunity related GTPase Q	0.68	0.01
I3LNK5_PIG	GSPT1	G1 to S phase transition 1	0.77	0.03
I3LS72_PIG	N/A	Uncharacterized protein	1.25	0.02
I3LUR7_PIG	COL6A3	Collagen type VI alpha chain 3	0.81	0.02
K7GRY0_PIG	UBA1	Ubiquitin-like modifier-activating enzyme 1	0.79	0.05
Q8WNW4_PIG	CTNNB1	Beta-catenin	0.81	0.05

(continued)

Table 1. Continued

Only BZ (12 proteins)				
Spot ID	*Gene name*	*Protein name*	*Ratio*	*P*
Q0QEM6_PIG	ATPB5	ATP synthase subunit beta	0.39	0
TPM1_PIG	TPM1	Tropomyosin alpha-1 chain	0.68	0.03
A1XQT6_PIG	MYL1	MLC1f	0.65	0.004
ACADM_PIG	ACADM	Medium-chain specific acyl-CoA dehydrogenase, mitochondrial	0.57	0.04
APOA1_PIG	APOA1	Apolipoprotein A-I	0.65	0.004
F1RK10_PIG	SUCLA2	Succinate CoA ligase [ADP-forming] subunit beta, mitochondrial	0.57	0.04
F1RK48_PIG	SRL	Sarcalumenin isoform X	1.42	0.04
F1RX37_PIG	FGB	Fibrinogen beta chain	0.57	0.04
F1S902_PIG	COMP	Cartilage oligomeric matrix protein	1.42	0.04
F1SG00_PIG	TPM2	Tropomyosin 2 beta	0.70	0.02
F1SMJ1_PIG	C7	Complement component C7	0.80	0.02
PLMN_PIG	PLG	Plasminogen	0.80	0.02

Only RV (31 proteins)				
Spot ID	*Gene name*	*Protein name*	*Ratio*	*P*
A4GWT6_PIG	N/A	Adiponectin	1.39	0.04
B6VNT8_PIG	ACTC1	Cardiac muscle alpha actin 1	0.73	0.02
C1PIG4_PIG	PRKAR2A	cAMP-dependent protein kinase regulatory subunit type II alpha	0.79	0.03
F1SNW4_PIG	MYL3	MYL3	0.81	0.05
gi|335281954	ARHGAP1	Rho GTPase-activating protein 1 isoform X2	0.74	0.02
gi|335294000	LOC100522692	3-hydroxybutyrate dehydrogenase type 2	2.00	0.02
I3LK59_PIG	ENO1	Enolase 1	0.69	0.02
Q2XVP5_PIG	MAPRE1	Microtubule-associated protein RP/EB family member 1	1.33	0.03
Q6V9B4_PIG	APM1	Adiponectin	1.28	0.01
Q9GMA9_PIG	SERPIN3-2	Alpha 1-antichymotrypsin 2	5.36/4.74	0.03/0.04
TPM3_PIG	TPM3	Tropomyosin alpha-3 chain	0.81	0.03
D3K5K2_PIG	FKBP4	Peptidylprolyl isomerase	0.77	0.05
DESM_PIG	DES	Desmin	1.44	0.03
F1REW9_PIG	DENR	Density-regulated protein	1.35	0.04
F1RGW0_PIG	PDIA2	Protein disulfide isomerase family A member 2	3.58	0.03
F1RQS2_PIG	CLIC5	Chloride intracellular channel protein	1.35	0.04
F1RZ96_PIG	TARSL2	Threonyl-tRNA synthetase like 2	1.82	0.03
F1S5Q3_PIG	MAPK9	Mitogen-activated protein kinase	0.81	0.04
F1SD87_PIG	FBLN5	Fibulin 5	1.24	0.05
F1SG41_PIG	ALDH1L2	10-formyltetrahydrofolate dehydrogenase	1.44	0.02
F1SIS9_PIG	NDUFA10	NADP dehydrogenase [ubiquinone] 1 alpha subcomplex subunit 10, mitochondrial	0.16	0.03
F1SJR7_PIG	TTLL12	Tubulin tyrosine ligase like 12	0.77	0.02
F1SS26_PIG	THBS1	Thrombospondin 1	1.30	0.03
F1SVB0_PIG	CAPG	Capping actin protein, gelsolin like	0.16	0.03
F2Z5J8_PIG	EIF2S1	Eukaryotic translation initiation factor 2 subunit 1	1.23	0.04
gi|47523796	ADIPOQ	Adiponectin precursor, C1Q and collagen domain containing	1.44	0.03

(continued)

Table 1. Continued

HS90A_PIG	HSP90AA1	Het shock protein 90-alpha	0.81	0.05
I3LD43_PIG	LAP3	Leucine aminopeptidase 3	1.44	0.03
I3LN84_PIG	LXN	Latexin	1.30	0.03
PALMD_PIG	PALMD	Palmdelphin	0.77	0.02
PLAK_PIG	Jup	Junction plakoglobin	0.76	0.01

LV-BZ (2 proteins)					
Spot ID		*Gene name*	*Protein name*	*Ratio*	*P*
gi|343962580	LV/BZ	ACTN2	Alpha actinin 2	0.81/0.82	0.05/0.02
HYES_PIG	LV/BZ	EPHX2	Bifunctional epoxide hydrolase 2	1.87/1.66	0.04/0.03

LV-RV (9 proteins)					
Spot ID		*Gene name*	*Protein name*	*Ratio*	*P*
Q9GMA6_PIG	LV	SERPINA3-2	Alpha 1-antichymotrypsin 2	0.18	0.02
	RV			5.36	0.03
E1CAJ5_PIG	LV/RV	grp-58	Protein-disulfide isomerase	1.45/2.37	0.03/0.03
F1RGJ2_PIG	LV/RV	CTNNA1	Catenin alpha 1	6.92/1.82, 1.48	0.01/0.03, 0.03
F1RHL9_PIG	LV	ACTN2	Actinin alpha 2	6.92, 0.72, 0.79	0.01, 0.02, 0.05
	RV			1.44, 1.82, 1.48	0.02, 0.03, 0.03
F1RT46_PIG	LV/RV	QRSL1	Glutamyl-tRNA (Gln) amidotransferase subunit A, mitochondrial	1.45/2.37	0.03/0.03
F1S1A8_PIG	LV/RV	NDUFS2	Uncharacterized protein	0.83/0.70	0.01/0.01
F1SU59_PIG	LV/RV	ANXA7	Annexin	0.83/0.70	0.01/0.01
G9F6X9_PIG	LV/RV	N/A	Dihydropyrimidinase-like 2	1.45/2.37	0.03/0.03
LMNA_PIG	LV/RV	LMNA	Pelamin A/C	0.83/0.70	0.01/0.01

LV-BZ-RV					
Spot ID		*Gene name*	*Protein name*	*Ratio*	*P*
K9J6H8_PIG	LV	A2M	Alpha-2-macroglobulin	1.87	0.04
	BZ			1.66	0.03
	RV			0.77, 0.77	0.04, 0.01

red: protein with induced expression; green: protein with repressed expression

LV: left ventricular; BZ: border zone; RV: right ventricular.

observed during the late phase of infarct healing, *formation of a mature scar. CASP3 and CASP4* (caspase-3 and -4), members of the pro-inflammatory family of caspases, are key mediators of apoptosis and inflammation, also during MI. The protein tyrosine phosphatase encoded by *PTPN13* exerts pro-apoptotic effects via IRS-1/PI3K/Akt signaling, while *PSRC1* specifies a proline-rich protein regulated by p53 and participates in p53/TP53-regulated growth suppression.[26] *NDFIP1* encodes a putative NFκB and MAPK-activating protein that controls cell growth and nuclear localization of *PTEN*, and thus cell division and survival. *NDFIP1* mutant mice suffered larger infarct sizes following cerebral ischemia,[27] and the gene product of *LAMP2* (lysosome-associated membrane protein 2) has been associated, e.g., with autophagy in skeletal muscle of infarcted rats.[28]

In this study, dronedarone increased mRNA amounts of *ATP2B4*, *ATP2B1*, *TRDN* and decreased that of *ATP2A2* after AMI. This is indicative of increased cytoplasmic Ca^{2+} levels, which may translate into elevated mitochondrial matrix Ca^{2+} levels, compromised OXPHOS, increased ROS levels, and cell death. Supporting this view, increased mRNA amounts of *PRDX1*, *GSTA4*, *GSTM3*, and *ENC1*, all encoding antioxidants and detoxification enzymes induced by elevated levels of ROS, were observed in BZ-D.

Table 2. Overlap of dronedarone-regulated genes in BZ observed in both transcriptome and proteome analysis.

Gene name	Protein description	Molecular function	mRNA-regulation factors	Protein-regulation factors
ADIPOQ	Adiponectin	Structural component (ECM)	1.52	1.20 (1.24, 1.18, 1.04)
COL6A1	Collagen α-1(VI) chain	Structural component (ECM)	1.58	1.74 (1.74, 1.64, 1.52, 1.36, 0.84, 0.84, 0.78, 0.72)
COMP	Cartilage oligomeric matrix protein		2.32	**1.42***
CALD1	Caldesmon	Structural component (cyto skeleton) Actin-binding	1.83	0.77 (0.87, 0.84, 0.76)
CAPG	Macrophage-capping Protein	Structural component (cyto skeleton) Ca^{2+}-binding	2.2	1.91 (0.76)
MRLC2	Myosin regulatory light chain 2, myocardial isoform	Structural component (cyto skeleton) Calcium-/calmodulin-binding	1.25	0,10
MYBPC3	Myosin-binding protein C, cardiac type	Proteinkinase Structural component (cyto skeleton) GTPase-regulator	0.74	0.82 (1.45, 1.20, 1.17, 1.16, 1.13, 1.09, 1.05)
PDLIM1	PDZ and LIM domain Protein 1	Transcription factor structural component (cyto skeleton) Actin-binding	1.81	0.79 (0.89, 0.86, **0.85***, 0.74)
TPM3	Tropomyosin α-3	Motor protein Structural component (cyto skeleton)	1.43	0.81 (1.04, 0.94, 0.91, 0.87)
ACADSB	Short/Branched-chain specific Acyl-CoA dehydrogenase, mitochondrial	Oxidoreductase Transferase	0.66	0.76 (1.02, 1.00, 1.00, 1.00)
BDH2	3-Hydroxybutyrat dehydrogenase Type 2		0.76	1.50 (1.26)
DPYSL3	Dihydropyrimidinase-related protein 3	Hydrolase	1.39	1.22 (1.12, 1.06, 1.00, 0.96)
EFHD2	EF-hand domain-containing protein D2	Ca^{2+}-binding	1.51	0,67
FTL	Ferritin light chain		1.32	0.73 (0.97)
HSPA5	78 kDa glucose-regulated Protein	Protein folding	1.31	4.55 (1.09, 0.94, 0.89, 0.83)
IGHM	Ig alpha-1 chain C		5.6	0.69 (0.96, 0.93, 0.89, 0.89, 0.85, 0.82)
MAPK9	Mitogen-activated Protein kinase 9	Protein kinase	1.43	1,92
NDUFA10	NADH Dehydrogenase 1 α-sub-complex UE 10, mitochondrial	Nucleotide kinase	0.63	0.63 (1.91, 1.21, 1.01)
PCCB	Propionyl-CoA carboxylase β-chain, mitochondrial	Ligase	0.6	1.31 (1.22, 1.02, 1.01)
PDIA3	Protein disulfide isomerase A3	Protein disulfide isomerase	1.23	8.41 (1.04, 0.41)
RAD23A	UV excision repair protein RAD23 Homolog	Damaged-DNA-binding	0.8	0,48
SERPINB9	Serpin B9	Serin protease Protease inhibitor	0.79	0,82
TGFBI	TGFβ-induced protein ig-h3	Receptor-binding	1.38	1,32

dark grey induced
light grey induced/repressed (multiple spots with contrary regulation to main spot)
middle grey repressed
white contrary regulation transcriptome/proteome
BZ: border zone.
* $p<0.01$ (all others: $p<0.05$).

Dronedarone's effects on the inflammatory phase of infarct healing were evidenced by significantly increased expression of *CXCL6*, *IL6*, *IL23R*, *HCK*, *CXCL9*, and *IL1R1* in BZ-D. Again, dronedarone lacked significant efficacy in MI, but partially changed *IL1R1 mRNA levels* (43.4% in MI-D). Eventually, the inflammatory phase is limited by anti-inflammatory counter-regulatory mechanisms to maintain tissue integrity and stability to a certain extent. In this context, the activity of matricellular proteins, ECM, and enzymes contributing in tissue remodeling is required to facilitate repair or even partial functional recovery. The results of *single omics* approaches and of the *integrated omics* approach in particular, identified a considerable number of such ECM and matricellular proteins as major targets of dronedarone. This view is strengthened by the fact that the top 10 IPA *Disease Charts* and *Tox Function Charts* affected by dronedarone are indeed related to cardiac remodeling and repair processes. Many of the underlying molecular targets do represent the transcriptome/proteome overlap or constitute the established integrated

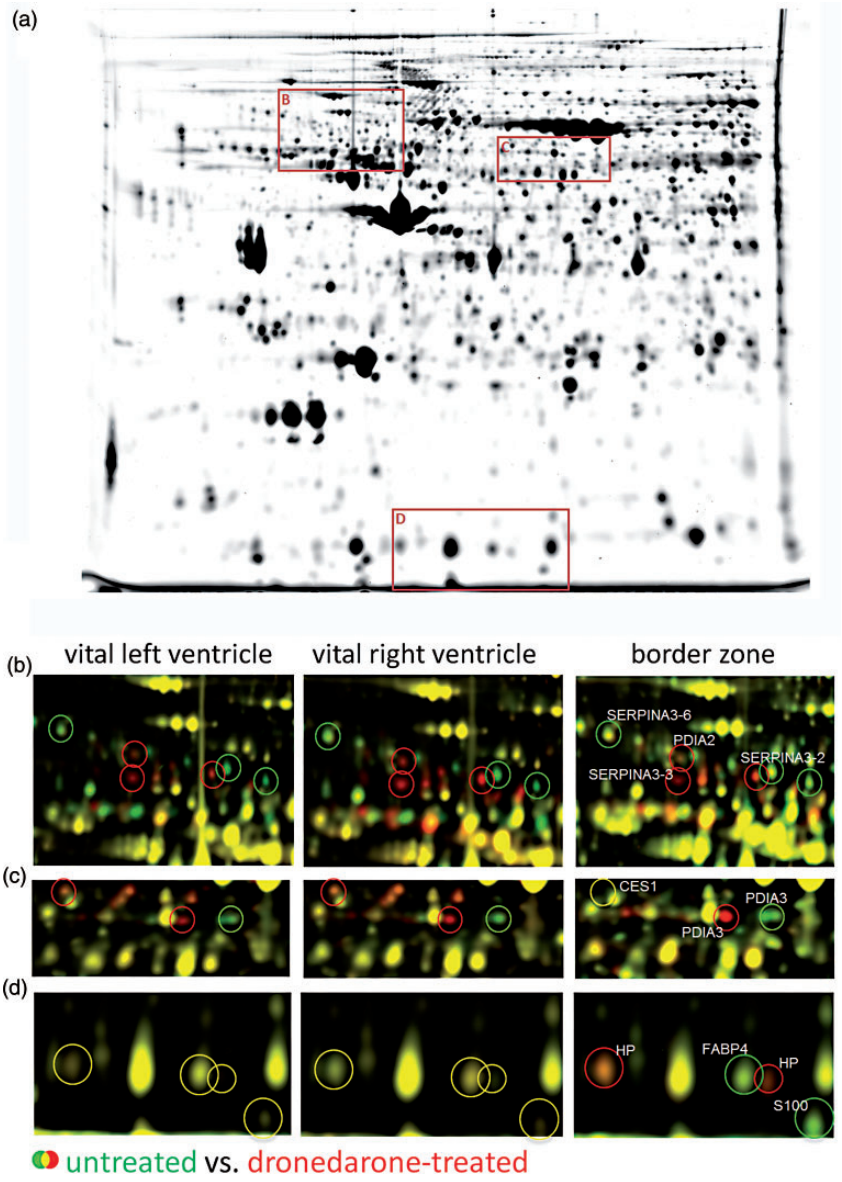

Figure 5. 2D-DIGE analysis: 2214 distinct protein spots were statistically analyzed by 2D-DIGE. Spots of interest were cut out, tryptically digested and identified by mass spectrometry. Dual channel overlays illustrate the dronedarone-mediated protein level changes in dronedarone-treated animals vs. untreated controls. (a) 2D-PAGE overview of separated proteins, regions of interest highlighted and displayed in dual channel overlays for each condition. (b) Changes in the protein levels of Serpin Isoforms and PDIA2. (c) Changes in the protein levels of CES1 and isoforms of PDIA3. (d) Changes in the protein levels of fatty acid-binding protein FABP4 and Ca-binding protein S100 (J9JIL5_PIG).

network (Online Supplement 1). The protein encoded by *TNFAIP6* (also known as TSG-6, tumor necrosis factor α-induced protein 6) gene is a multifunctional 35 kDa glyco-protein and a member of the hyaluronate-binding protein family (hyaladherins). Its over-expression limits inflammatory responses in many pathological settings including MI. Here, significantly elevated mRNA amounts of *TNFAIP6* (3.39-fold) were observed in BZ-D, and dronedarone attenuated its expression in MI (34.6% increase in MI-D). Hyaladherins are involved in ECM stability and cell migration.[29] Recombinant TNFAIP6 reduced inflammation and infarct size in experimental AMI.[30] Other genes encoding anti-inflammatory and immunosuppressive cytokines that were significantly induced by dronedarone included *TGFB3* (transforming growth factor-beta isoform 3) and *IL27ra* (interleukin 27 receptor alpha). The latter protein mediates anti-inflammatory effects via JAK/STAT signaling. Notably, a significant increase in *STAT3* mRNA was observed in BZ-D.

TGF-β, a potent anti-inflammatory cytokine, functions as "master switch" for transition from inflammation to fibrosis. Intracellular Ca^{2+} levels regulate TGF-β signaling. The levels of matricellular protein-coding transcript, thrombospondin (TSP/THBS)-1, a key activator of TGF-β, were induced in BZ-D and partially affected in MI-D.[31] Thrombospondins, *THBS1* in particular, crucially affect maturation of the infarct scar and prevent expansion of MI.[31] *THBS1* expression is elevated during early phases of cardiac healing. By activating *TGFB1*, *THBS1* suppresses inflammatory chemokines/cytokines and prevents leakage

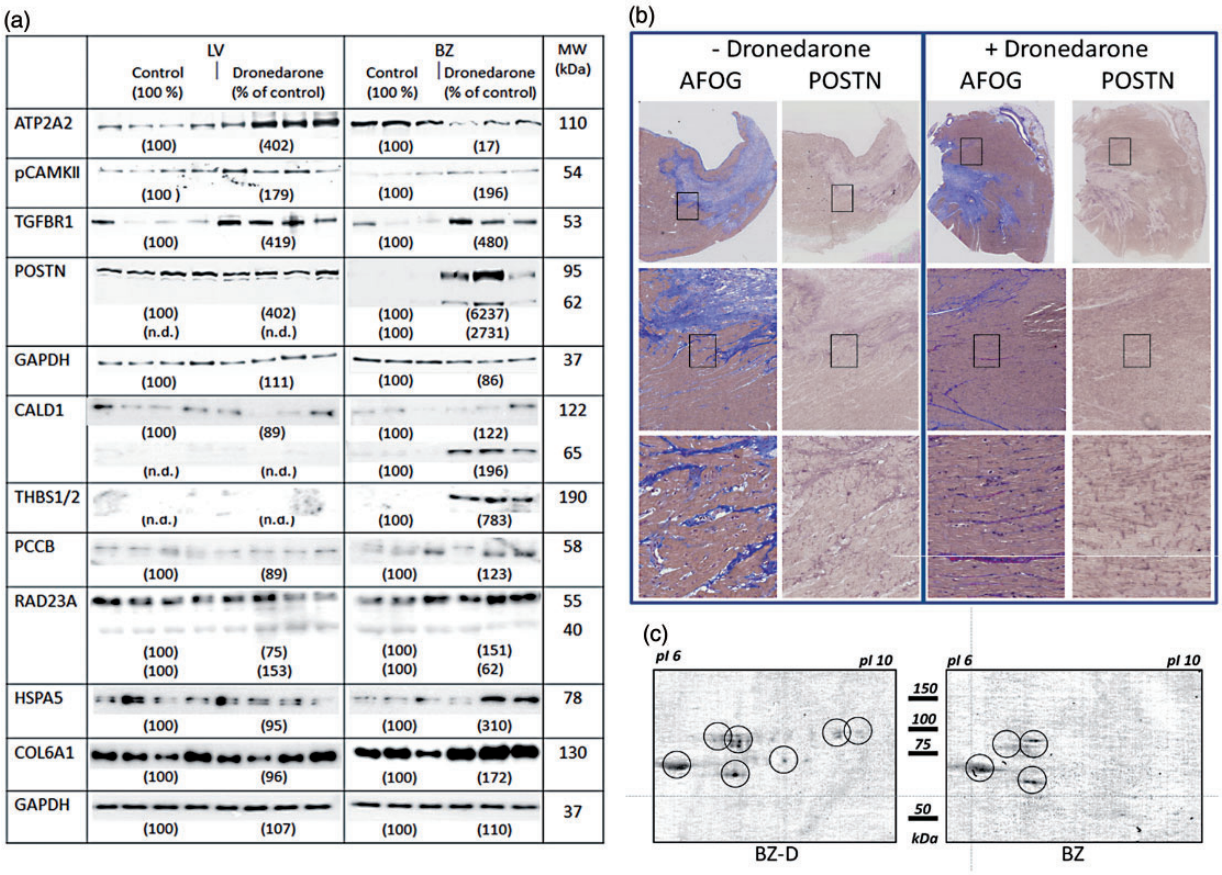

Figure 6. (a) Immunoblot analysis demonstrating the effect of dronedarone on ATP2A2 (SERCA), pCAMKII, COL6A1, TGFBR1, and POSTN levels in the LV and BZ. In the BZ, there is a substantial increase of POSTN in response to dronedarone. GAPDH was used as loading control. (b) Immunohistochemical detection of POSTN in cardiac tissue slices of dronedarone-treated (right panel) or control pigs (left panel). AFOG staining was used to visualize fibrosis (blue area) and vital myocardiocytes (yellow cells). No differences in infarct size were noted. (c) Immunodetection of POSTN in 2D-immunoblot analysis (pH 6–10; MW 50–150 kDa) revealing dronedarone-dependent increase in spot intensities (95 and 68 kDa, approximately).

of inflammatory process into the non-infarcted region.[32] *THBS2* encoded protein is secreted predominantly by fibroblasts and shows strongest induction during later stages of post-infarct healing. Although not activating *TGFB1*, *THBS2* crucially determinates integrity of ECM during scar maturation. *THBS2*$^{-/-}$ mice are prone to cardiac rupture after MI due to abnormal collagen fibrillogenesis.[33] TGFB1 stimulates the transformation of fibroblasts into activated fibroblasts or myofibroblasts that proliferate and secrete ECM for scar formation. Interestingly, the genes encoding SMAD2, a key downstream modulator of BMP/TGFβ-signaling, and SMURF1, an ubiquitin-ligase that is specific for receptor-regulated SMAD proteins, were substantially induced in BZ-D, with partial impact also in MI-D. TGFB1 and fibroblast growth factor-2 (FGF2) synergistically enhance ECM production. FGF2/FGFR2 protects ischemic and/or infarcted myocardium.[34] We observed an increased expression *of FGFR2* in BZ-D.

TGF-β isoforms, upon activation by THBS1 and binding to the receptor, lead to the phosphorylation of SMAD2/3 and subsequent dimerization with SMAD4. This activates ECM gene expression. We demonstrate increased expression of characteristic myofibroblast genes, including *POSTN*, *FN1*, *CTGF*, and *TNC* encoding periostin, fibronectin, connective tissue growth factor, and tenascin-C, respectively, as well as of *SPARC* encoding secreted protein, acidic and rich in cysteine (*alias* osteonectin). More than half of dronedarone-regulated target genes belong to *Formation of the mature scar* and *ECM stimulation* phases, and are constituents of *Disease Charts* and *Tox Function Charts* and, therefore, of the integrated network. Again, this suggests that genes encoding ECM members and matricellular proteins, such as *COL8A1, TNN, GPNMB, LMNA, ACAN, COL1A2, VCAN, COMP, COL8A1, COL12A1, COL6A1, COL16A1, COL5A1, COL5A2,* and *COL1A1*, contribute to dronedarone-dependent alterations of structure and stability of repaired myocardium and/or scar tissue. Of note, collagens 6A1, 6A2, and 6A3 were identified as regulated at the proteome level and COL6A1 and COLA3 are even constituents of the "overlap" (transcriptome 1.5-fold, $P < 0.05$; proteome 1.2-fold, $P < 0.05$). This assignment to the "overlap" together with the high abundancy of various collagens in the resulting "integrated network" (collagens I, III, IV, V, VI, VIII, XII; Online Supplement 1 and 2) identifies these collagens and other matricellular proteins as "major" (key targets) dronedarone-regulated targets.

A marked but transient up-regulation of *TNC* and *FN1* in the infarct area has been reported during the proliferative phase of healing.[35] The protein encoded by *SPARC* regulates infarction healing and collagen maturation by

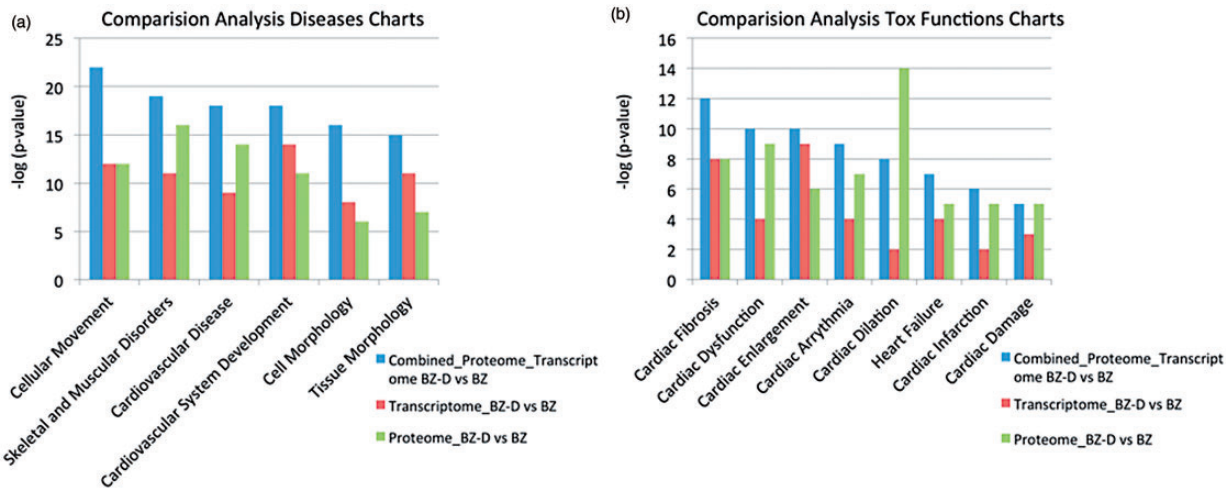

Figure 7. IPA comparison analysis – integrated analysis of combined transcriptome and proteome data compared to each single approach increases prediction *P*-values significantly for disease (a) and Tox function (b) charts. The presented cardiac associated diseases (6 out of 10) and Tox functions (8 out of 10) have been selected from the top 10 IPA results.

direct interaction with collagen type I fibers or by interference with the assembly of fibronectin into fibrils. In our study, *ITGAV*, *ITGA8*, *ITGBL1*, and *ITGB3* encoding integrin subunits were induced in response to AMI, where *ITGA8* was significantly induced in BZ-D.

Accumulating evidence establishes periostin encoded by *POSTN* as a crucial player in chronic cardiac remodeling after MI.[23,36,37] Periostin which contains four fasciclin domains, promotes cellular adhesion and movement and collagen fibrillogenesis. It modulates collagen deposition, fibrosis, and scar mechanics.[38] Of note, these processes are fully covered in the top *Disease Charts* and *Tox Function Charts* that have been identified by the combined omics approach. Decreased periostin plasma levels were associated with AMI,[39] but the protein promotes cardiac repair after MI as indicated by improved ventricular remodeling and myocardial function, reduced fibrosis and infarct size, as well as increased angiogenesis.[40,41]

POSTN$^{-/-}$ mice exhibit impaired cardiac healing and increased mortality after AMI because of cardiac rupture due to reduced myocardial stiffness and impaired collagen formation.[36,42] Paradoxically, surviving *POSTN*-deficient mice show less fibrosis and improved cardiac performance.[36,42] These data imply that periostin might be essential for post-AMI cardiac healing.

Dronedarone could affect periostin-dependent cardiac healing and remodeling after AMI by different, potentially overlapping, mechanisms. Firstly, periostin might regulate the integrity of the ECM through its ability to bind multiple ECM proteins, such as those encoded by *TNC* and *FN1* as well as collagen V, collagen I, aggrecan, and heparin, thereby affecting the structural integrity of the heart matrix or stretch-sensitive signaling.[43,44] This view is supported by short sized, disorganized and less efficiently cross-linked collagen fibrils and disorganized ECM in *POSTN*-deficient mice.[45,46] In addition, periostin promotes collagen cross-linking through BMP1-mediated proteolytic activation of LOX on the extracellular matrix.[44] Thus, by altering the composition and performance of the ECM, periostin affects cardiac healing and remodeling after MI. Secondly, periostin could modulate adhesion-dependent signaling by binding to the integrins αvβ3, αvβ5, and α4β6 and transducing signals into the infarct region that activate migration of cardiac fibroblasts through FAK phosphorylation. Migrated cells differentiate into αSMA-positive fibroblasts and contribute to strengthening of the wall stiffness through collagen synthesis and changes of collagen cross-linking and quality.[40,42,45] Recent data imply that different isoforms of periostin function to regulate reactive fibrosis in remote regions and replacement fibrosis in infarct tissue in a distinct manner.[46,47] This might explain some inconsistent results that have been obtained in previous studies. Dronedarone increased *POSTN* mRNA levels in both healthy LV and BZ. In the BZ, dronedarone led to a substantial increase of periostin protein in immunoblot analysis. This increase was not observed by immunohistochemical analysis of cardiac tissue slices. The hypothesis that this discrepancy is due to dronedarone-dependent protein modifications was supported by the alterations of periostin mobility observed in 2D analysis.

Dronedarone was developed as an antiarrhythmic drug and, thus, might affect ion channel expression. Indeed, a very recent study demonstrates increased protein expression of KIR2.1 in response to dronedarone which results from impaired backward trafficking and decreased degradation.[48] Accordingly, mRNA levels were not altered by dronedarone.[48] The observed increase in mRNA levels of *KCNMA1*, *KCNE1*, *KCNQ1*, *KCNH2* provoked by dronedarone in our study (Online Supplement 6), therefore seems to reflect an increase in the fraction of cardiomyocytes in the tissue rather than an induction of gene expression.

The present study has some limitations. First, analyses have been performed at one time point only. The consistent results obtained by transcriptomics, proteomics, and also of combined omics identified significant expression changes that exist at this particular time point, at least in the BZ. Future studies may apply single or combined omics to

evaluate dronedarone's effects on gene/protein expression in a temporal manner. Second, this study is focused on the identification of the molecular targets and signaling hubs that underlie the previously observed effects of dronedarone on microcirculation and infarct size. To this end, a hypothesis-free and unbiased "integrated omics" approach has been applied here. The effects on cardiac electrophysiology and function, and long-term effects on stability and contractility in particular, remain to be addressed in future work.

Conclusions

In summary, our data indicate pronounced efficacy of dronedarone in the infarct border-zone. In the infarct area, dronedarone, although less effective, still showed partial impact on gene expression. However, there are no experimental hints that dronedarone *per se* has direct harmful effects after induced myocardial infarction in ventricular tissue.

By applying integrated omics analysis, *Disease Charts* and *Tox Function Charts* were identified, that associate dronedarone with different cellular/cardiac processes that are employed in, e.g., post-infarction cardiac healing and remodeling processes. Specifically, dronedarone exerted strong effects on the expression of matricellular proteins and ECM, which could explain its impact on among others cardiac fibrosis, cardiac dysfunction, and cardiac infarction as well as cellular movement and cell morphology. This view is supported by the results of an integrated network analysis, which illustrates dronedarone's capability of orchestrating factors and processes of cardiac remodeling and repair. To what extent dronedarone can improve cardiac functionality in the long term, remains to be assessed in future studies. The long-term consequences of dronedarone treatment on cardiac stability and function need to be elucidated fully.

Authors' contributions: AG and UL designed the study. RKC, KU, AB, CW, JL, UL, CS, KD, BP, and MS conducted the experiments. RKC, JL, UL and CS drafted the manuscript. All authors participated in interpretation of the studies and analysis of the data and review of the manuscript.

ACKNOWLEDGEMENTS

We thank Manja Möller, Ines Schultz, and Marc Niemeyer for the excellent technical assistance.

DECLARATION OF CONFLICTING INTERESTS

The author(s) declared no potential conflicts of interest with respect to the research, authorship, and/or publication of this article.

FUNDING

The author(s) disclosed receipt of the following financial support for the research, authorship, and/or publication of this article: We are grateful to Sanofi-Aventis for the financial support of this investigator sponsored trial.

ORCID iD

Christian Scharf http://orcid.org/0000-0001-6806-6450
Uwe Lendeckel http://orcid.org/0000-0002-0684-9959

REFERENCES

1. Hohnloser SH, Crijns HJGM, van Eickels M, Gaudin C, Page RL, Torp-Pedersen C, Page RL, Torp-Pedersen C, Connolly SJ. ATHENA Investigators. Effect of dronedarone on cardiovascular events in atrial fibrillation. *N Engl J Med* 2009;**360**:668–78
2. Pisters R, Hohnloser SH, Connolly SJ, Torp-Pedersen C, Naditch-Brûlé L, Page RL, Crijns HJ. ATHENA Investigators. Effect of dronedarone on clinical end points in patients with atrial fibrillation and coronary heart disease: insights from the ATHENA trial. *Europace* 2014;**16**:174–81
3. Køber L, Torp-Pedersen C, McMurray JJV, Gøtzsche O, Lévy S, Crijns H, Amlie J, Carlsen J, Dronedarone Study Group. Increased mortality after dronedarone therapy for severe heart failure. *N Engl J Med* 2008;**358**:2678–87
4. Connolly SJ, Camm AJ, Halperin JL, Joyner C, Alings M, Amerena J, Atar D, Avezum Á, Blomström P, Borggrefe M, Budaj A, Chen SA, Ching CK, Commerford P, Dans A, Davy JM, Delacrétaz E, Di Pasquale G, Diaz R, Dorian P, Flaker G, Golitsyn S, Gonzalez-Hermosillo A, Granger CB, Heidbüchel H, Kautzner J, Kim JS, Lanas F, Lewis BS, Merino JL, Morillo C, Murin J, Narasimhan C, Paolasso E, Parkhomenko A, Peters NS, Sim KH, Stiles MK, Tanomsup S, Toivonen L, Tomcsányi J, Torp-Pedersen C, Tse HF, Vardas P, Vinereanu D, Xavier D, Zhu J, Zhu JR, Baret-Cormel L, Weinling E, Staiger C, Yusuf S, Chrolavicius S, Afzal R, Hohnloser SH, PALLAS Investigators. Dronedarone in high-risk permanent atrial fibrillation. *N Engl J Med* 2011;**365**:2268–76
5. Miyasaka Y, Barnes ME, Gersh BJ, Cha SS, Bailey KR, Seward JB, Iwasaka T, Tsang TS. Coronary ischemic events after first atrial fibrillation: risk and survival. *Am J Med* 2007;**120**:357–63
6. Saito D, Haraoka S, Ueda M, Fujimoto T, Yoshida H, Ogino Y. Effect of atrial fibrillation on coronary circulation and blood flow distribution across the left ventricular wall in anesthetized open-chest dogs. *Jpn Circ J* 1978;**42**:417–23
7. Wichmann J, Ertl G, Rudolph G, Kochsiek K. Effect of experimentally induced atrial fibrillation on coronary circulation in dogs. *Basic Res Cardiol* 1983;**78**:473–91
8. Raddino R, Poli E, Pelà G, Gargano M, Manca C. Inhibitory actions of amiodarone on the isolated rabbit heart and aorta. *Gen Pharmacol* 1989;**20**:313–7
9. Guiraudou P, Pucheu SC, Gayraud R, Gautier P, Roccon A, Herbert JM, Nisato D. Involvement of nitric oxide in amiodarone- and dronedarone-induced coronary vasodilation in guinea pig heart. *Eur J Pharmacol* 2004;**496**:119–27
10. Bukowska A, Hammwöhner M, Sixdorf A, Schild L, Wiswedel I, Röhl F-W, Wolke C, Lendeckel U, Aderkast C, Bochmann S, Chilukoti RK, Mostertz J, Bramlage P, Goette A. Dronedarone prevents microcirculatory abnormalities in the left ventricle during atrial tachypacing in pigs. *Br J Pharmacol* 2012;**166**:964–80
11. Skyschally A, Heusch G. Reduction of myocardial infarct size by dronedarone in pigs – a pleiotropic action? *Cardiovasc Drugs Ther* 2011;**25**:197–201
12. Engelhorn T, Schwarz MA, Heusch G, Doerfler A, Schulz R. Reduction of cerebral infarct size by dronedarone. *Cardiovasc Drugs Ther* 2011;**25**:523–9
13. Linke J, Utpatel K, Wolke C, Evert M, Kühn JP, Bukowska A, Wolke C, Lendeckel U, Aderkast C, Bochmann S, Chilukoti RK, Mostertz J, Bramlage P, Goette A. Dronedarone does not affect infarct volume assessed by MRT in a porcine model of myocardial infarction. *Mol Med Rep* 2015;**12**:5169–78
14. Couture O, Callenberg K, Koul N, Pandit S, Younes R, Hu Z-L, Dekkers J, Reecy J, Honavar V, Tuggle C. ANEXdb: an integrated animal annotation and microarray expression database. *Mamm Genome* 2009;**20**:768–77

15. Chilukoti RK, Mostertz J, Bukowska A, Aderkast C, Felix SB, Busch M, Völker U, Goette A, Wolke C, Homuth G, Lendeckel U. Effects of irbesartan on gene expression revealed by transcriptome analysis of left atrial tissue in a porcine model of acute rapid pacing in vivo. *Int J Cardiol* 2013;**168**:2100–8
16. Chilukoti RK, Giese A, Malenke W, Homuth G, Bukowska A, Goette A, Felix SB, Kanaan J, Wollert HG, Evert K, Verheule S, Jais P, Hatem SN, Lendeckel U, Wolke C. Atrial fibrillation and rapid acute pacing regulate adipocyte/adipositas-related gene expression in the atria. *Int J Cardiol* 2015;**187**:604–13
17. Junker H, Venz S, Zimmermann U, Thiele A, Scharf C, Walther R. Stage-related alterations in renal cell carcinoma–comprehensive quantitative analysis by 2D-DIGE and protein network analysis. *PLoS One* 2011;**6**:e21867
18. Thiele T, Steil L, Gebhard S, Scharf C, Hammer E, Brigulla M, Lubenow N, Clemetson KJ, Völker U, Greinacher A. Profiling of alterations in platelet proteins during storage of platelet concentrates. *Transfusion* 2007;**47**:1221–33
19. Nishtala K, Phong TQ, Steil L, Sauter M, Salazar MG, Kandolf R, Felix SB, Völker U, Klingel K, Hammer E. Proteomic analyses of age related changes in A.BY/SnJ mouse hearts. *Proteome Sci* 2013;**11**:29
20. Lendeckel D, Eymann C, Emicke P, Daeschlein G, Darm K, O'Neil S, Beule AG, von Woedtke T, Völker U, Weltmann KD, Jünger M, Hosemann W, Scharf C. Proteomic changes of tissue-tolerable plasma treated airway epithelial cells and their relation to wound healing. *Biomed Res Int* 2015; **2015**: 506059.
21. Hammer E, Phong TQ, Steil L, Klingel K, Salazar MG, Bernhardt J, Kandolf R, Kroemer HK, Felix SB, Völker U. Viral myocarditis induced by Coxsackievirus B3 in A.BY/SnJ mice: analysis of changes in the myocardial proteome. *Proteomics* 2010;**10**:1802–18
22. Cima I, Schiess R, Wild P, Kaelin M, Schüffler P, Lange V, Picotti P, Ossola R, Templeton A, Schubert O, Fuchs T, Leippold T, Wyler S, Zehetner J, Jochum W, Buhmann J, Cerny T, Moch H, Gillessen S, Aebersold R, Krek W. Cancer genetics-guided discovery of serum biomarker signatures for diagnosis and prognosis of prostate cancer. *Proc Natl Acad Sci U S A* 2011;**108**:3342–7
23. Matsui Y, Morimoto J, Uede T. Role of matricellular proteins in cardiac tissue remodeling after myocardial infarction. *World J Biol Chem* 2010;**1**:69–80
24. Opie LH, Commerford PJ, Gersh BJ, Pfeffer MA. Controversies in ventricular remodelling. *Lancet* 2006;**367**:356–67
25. White HD, Norris RM, Brown MA, Brandt PW, Whitlock RM, Wild CJ. Left ventricular end-systolic volume as the major determinant of survival after recovery from myocardial infarction. *Circulation* 1987;**76**:44–51
26. Dun B, Sharma A, Xu H, Liu H, Bai S, Zeng L, She JX. Transcriptomic changes induced by mycophenolic acid in gastric cancer cells. *Am J Transl Res* 2013;**6**:28–42
27. Howitt J, Lackovic J, Low L-H, Naguib A, Macintyre A, Goh CP, Callaway JK, Hammond V, Thomas T, Dixon M, Putz U, Silke J, Bartlett P, Yang B, Kumar S, Trotman LC, Tan SS. Ndfip1 regulates nuclear PTEN import in vivo to promote neuronal survival following cerebral ischemia. *J Cell Biol* 2012;**196**:29–36
28. Jannig PR, Moreira JBN, Bechara LRG, Bozi LHM, Bacurau AV, Monteiro AWA, Dourado PM, Wisløff U, Brum PC. Autophagy signaling in skeletal muscle of infarcted rats. *PLoS One* 2014;**9**:e85820
29. Day AJ, Milner CM. TSG-6: a multifunctional protein with anti-inflammatory and tissue-protective properties. *Matrix Biol* 2018; pii: S0945-053X(17)30473-0. Epub ahead of print.
30. Lee RH, Pulin AA, Seo MJ, Kota DJ, Ylostalo J, Larson BL, Semprun-Prieto L, Delafontaine P, Prockop DJ. Intravenous hMSCs improve myocardial infarction in mice because cells embolized in lung are activated to secrete the anti-inflammatory protein TSG-6. *Cell Stem Cell* 2009;**5**:54–63
31. Murphy-Ullrich JE, Poczatek M. Activation of latent TGF-β by thrombospondin-1: mechanisms and physiology. *Cytokine Growth Factor Rev* 2000;**11**:59–69
32. Frangogiannis NG, Ren G, Dewald O, Zymek P, Haudek S, Koerting A, Winkelmann K, Michael LH, Lawler J, Entman ML. Critical role of endogenous thrombospondin-1 in preventing expansion of healing myocardial infarcts. *Circulation* 2005;**111**:2935–42
33. Kyriakides TR, Zhu YH, Smith LT, Bain SD, Yang Z, Lin MT, Danielson KG, Iozzo RV, LaMarca M, McKinney CE, Ginns EI, Bornstein P. Mice that lack thrombospondin 2 display connective tissue abnormalities that are associated with disordered collagen fibrillogenesis, an increased vascular density, and a bleeding diathesis. *J Cell Biol* 1998;**140**:419–30
34. Matsunaga S, Okigaki M, Takeda M, Matsui A, Honsho S, Katsume A, Kishita E, Che J, Kurihara T, Adachi Y, Mansukhani A, Kobara M, Matoba S, Tatsumi T, Matsubara H. Endothelium-targeted overexpression of constitutively active FGF receptor induces cardioprotection in mice myocardial infarction. *J Mol Cell Cardiol* 2009;**46**:663–73
35. Willems IE, Arends JW, Daemen MJ. Tenascin and fibronectin expression in healing human myocardial scars. *J Pathol* 1996;**179**:321–5
36. Oka T, Xu J, Kaiser RA, Melendez J, Hambleton M, Sargent MA, Lorts A, Brunskill EW, Dorn GW 2nd, Conway SJ, Aronow BJ, Robbins J, Molkentin JD. Genetic manipulation of periostin expression reveals a role in cardiac hypertrophy and ventricular remodeling. *Circ Res* 2007;**101**:313–21
37. Minicucci M, Santos P, Rafacho B, Goncalves A, Ardisson L, Batista D, Azevedo PS, Polegato BF, Okoshi K, Pereira EJ, Paiva SA, Zornoff LA. Periostin as a modulator of chronic cardiac remodeling after myocardial infarction. *Clinics* 2013;**68**:1344–9
38. Conway SJ, Molkentin JD. Periostin as a heterofunctional regulator of cardiac development and disease. *Curr Genomics* 2008;**9**:548–55
39. Cheng C-W, Wang C-H, Lee J-F, Kuo L-T, Cherng W-J. Levels of blood periostin decrease after acute myocardial infarction and are negatively associated with ventricular function after 3 months. *J Investig Med* 2012;**60**:523–8
40. Kühn B. del Monte F, Hajjar RJ, Chang Y-S, Lebeche D, Arab S, Keating MT. Periostin induces proliferation of differentiated cardiomyocytes and promotes cardiac repair. *Nat Med* 2007;**13**:962–9
41. Ladage D, Yaniz-Galende E, Rapti K, Ishikawa K, Tilemann L, Shapiro S, Takewa Y, Muller-Ehmsen J, Schwarz M, Garcia MJ, Sanz J, Hajjar RJ, Kawase Y. Stimulating myocardial regeneration with periostin Peptide in large mammals improves function post-myocardial infarction but increases myocardial fibrosis. *PLoS One* 2013;**8**:e59656
42. Shimazaki M, Nakamura K, Kii I, Kashima T, Amizuka N, Li M, Saito M, Fukuda K, Nishiyama T, Kitajima S, Saga Y, Fukayama M, Sata M, Kudo A. Periostin is essential for cardiac healing after acute myocardial infarction. *J Exp Med* 2008;**205**:295–303
43. Norris RA, Damon B, Mironov V, Kasyanov V, Ramamurthi A, Moreno-Rodriguez R, Trusk T, Potts JD, Goodwin RL, Davis J, Hoffman S, Wen X, Sugi Y, Kern CB, Mjaatvedt CH, Turner DK, Oka T, Conway SJ, Molkentin JD, Forgacs G, Markwald RR. Periostin regulates collagen fibrillogenesis and the biomechanical properties of connective tissues. *J Cell Biochem* 2007;**101**:695–711
44. Maruhashi T, Kii I, Saito M, Kudo A. Interaction between periostin and BMP-1 promotes proteolytic activation of lysyl oxidase. *J Biol Chem* 2010;**285**:13294–303
45. Kim BR, Jang IH, Shin SH, Kwon YW, Heo SC, Choi E-J, Lee JS, Kim JH. Therapeutic angiogenesis in a murine model of limb ischemia by recombinant periostin and its fasciclin I domain. *Biochim Biophys Acta* 2014;**1842**:1324–32
46. Taniyama Y, Katsuragi N, Sanada F, Azuma J, Iekushi K, Koibuchi N, Okayama K, Ikeda-Iwabu Y, Muratsu J, Otsu R, Rakugi H, Morishita R. Selective blockade of periostin exon 17 preserves cardiac performance in acute myocardial infarction. *Hypertension* 2016;**67**:356–61
47. Morita H, Komuro I. Periostin isoforms and cardiac remodeling after myocardial infarction: is the dispute settled? *Hypertension* 2016; **67**:504–5
48. Ji Y, Takanari H, Qile M, Nalos L, Houtman MJC, Romunde FL, Heukers R, van Bergen En Henegouwen PMP, Vos MA, van der Heyden MAG. Class III antiarrhythmic drugs amiodarone and dronedarone impair KIR2.1 backward trafficking. *J Cell Mol Med* 2017;**21**:2514–23

(Received March 29, 2018, Accepted June 18, 2018)